

Antiferromagnetic coupling and enhanced magnetization in all-ferromagnetic superlattices

P. Padhan and W. Prellier

*Laboratoire CRISMAT, UMR CNRS 6508, 6,
Bld. du Maréchal Juin, F-14050 Caen, France*

R.C. Budhani

Department of Physics, Indian Institute of Technology, Kanpur 208016, India

(Dated: July 18, 2018)

Abstract

The structural and magnetic properties of a series of superlattices consisting of two ferromagnetic metals $\text{La}_{0.7}\text{Sr}_{0.3}\text{MnO}_3$ (LSMO) and SrRuO_3 (SRO) grown on (001) oriented SrTiO_3 are studied. Superlattices with a fixed LSMO layer thickness of 20 unit cells (u.c.) and varying SRO layer thickness show a sudden drop in magnetization on cooling through temperature where both LSMO and SRO layers are ferromagnetic. This behavior suggests an antiferromagnetic coupling between the layers. In addition, the samples having thinner SRO layers ($n < 6$) exhibit enhanced saturation magnetization at 10 K. These observations are attributed to the possible modification in the stereochemistry of the Ru and Mn ions in the interfacial region.

PACS numbers:

Transition metal oxides are used to design artificial magnetic structures with different bilayer configurations consisting of ferromagnetic (FM) - antiferromagnetic (AFM), AFM - AFM, and FM - FM thin films. On several combinations of FM-AFM bilayers the magnetic behavior exhibit horizontal and vertical hysteresis loop shifts,^{1,2,3,4} while some AFM-AFM bilayer systems show unexpected ferromagnetic behavior.^{5,6,7} Ke *et. al.*⁸ have observed exchange bias effects in multilayers consisting of FM-FM bilayers composed of $\text{La}_{0.67}\text{Sr}_{0.33}\text{MnO}_3$ and SrRuO_3 . While Uozu *et. al.*⁹ have observed an antiferromagnetic exchange coupling in the FM trilayer consisting of $\text{Sr}_{0.7}\text{Ca}_{0.3}\text{RuO}_3$ (SCRO) and $\text{La}_{0.6}\text{Sr}_{0.4}\text{MnO}_3$. in order to understand the coupling between the Ru and Mn ions at the interfaces of the two FM media, we have synthesized a series of superlattices consisting of FM-FM bilayers of $\text{La}_{0.67}\text{Sr}_{0.33}\text{MnO}_3$ (LSMO) and SrRuO_3 (SRO), where the LSMO layer thickness (d_{LSMO}) is fixed (~ 20 u.c.) and the SRO layer thickness (d_{SRO}) is varied. We note that the temperature dependence of magnetization of these superlattices strongly varies with the SRO layer thickness when the d_{SRO} is less than 6 unit cells. In addition, these superlattices show a sudden drop in magnetization at a temperature where both LSMO and SRO layers are ferromagnetic. The reproducible zero-field-cooled (ZFC) magnetic minor hysteresis loop shape in the field-cooled (FC) state of these superlattices suggests the existence of antiferromagnetic exchange coupling but not the presence of an interfacial layer of antiferromagnetic character.

Thin films of LSMO and SRO and their superlattices were grown on (001) oriented SrTiO_3 (STO) substrates at 720°C in oxygen ambient of 300 mTorr using a multitarget pulsed laser deposition technique. The deposition rates (typically ~ 0.26 Å/pulse and ~ 0.31 Å/pulse) of SRO and LSMO respectively were calibrated individually for each laser pulse of energy density ~ 3 J/cm². The chamber was filled with oxygen of 300 Torr after completion of deposition and then the samples were cooled to room temperature at the rate of $15^\circ\text{C}/\text{min}$. The superlattice structures were synthesized by repeating 15 times the bilayer consisting of a 20- unit cells thick LSMO layer and n- unit cells thick SRO layer, with n taking integer values from 1 to 12. In all multilayer samples, the bottom and top layers are of LSMO. Characterization of the structure and epitaxial nature of the multilayer and single layer films were performed using x-ray diffraction (XRD). For the magnetization (M) measurements, we have used a superconducting quantum interference device based magnetometer (Quantum Design MPMS-5). These measurements were carried out by cooling the sample to the desired temperature in the presence/absence of a magnetic fields applied along the [100] and [001]

directions of the STO substrate. The orientation of the magnetic field during the field-cooled measurements remained the same.

The lattice parameter of cubic STO (3.905 Å) is smaller than that of the pseudocubic lattice parameter of SRO (3.93 Å) but larger than that of the LSMO (3.88 Å). Thus, STO provides in-plane tensile stress for the epitaxial growth of LSMO with a lattice mismatch of -0.64 %. Similarly, it is expected that the LSMO would provides in-plane compressive stress for the epitaxial growth of SRO with a lattice mismatch 1.28 %. However, the LSMO-SRO superlattice stabilizes pseudocubic phases of these perovskites. In the conventional Θ -2 Θ scans of the superlattices, no peaks were observed other than the (00l) Bragg reflections of the constituents, the substrate and the satellites due to chemical modulation present in the multilayer. To evaluate the film thickness of LSMO and SRO layers, we have carried out quantitative refinement of the Θ -2 Θ scan of the trilayer structures using DIFFaX program.¹⁰ The experimental Θ -2 Θ scans and the simulated profiles of the two samples recorded around the (001) reflection of STO are shown in Fig. 1. The simulated profile using the calibrated thickness is in good agreement with the position of the Kiessig fringes and their relative intensity ratio confirming the quality of the layers.

LSMO exhibits positive spin polarization and ferromagnetic ordering with a relatively high Curie temperature ($T_C \sim 360$ K), small magnetic anisotropy and low coercive field (H_C).¹¹ While SRO shows negative spin polarization with a relatively small T_C (~ 150 K), strong uniaxial crystalline anisotropy and relatively large H_C .¹² In the magnetic multilayers discussed here the thickness of the LSMO layer is fixed at 20 u.c. A typical field-cooled temperature-dependence magnetization $M(T)$ for ~ 20 u.c. thick LSMO and SRO films is shown in the Fig. 2a and 2b, respectively. These relatively thin films of LSMO and SRO show a reduced T_C of ~ 330 K and ~ 145 K respectively. The reduced T_C seen in both the cases is due to finite size effect resulting from the strains.¹³

Fig. 3 displays the field-cooled (FC) magnetization of the superlattices with $n=2, 4, 5, 6$ and 7 . These measurements were performed at 0.01 tesla field applied along the out-of-plane direction of the STO. From this figure it appears that the alternative stacking of LSMO and SRO in a superlattice changes the $M(T)$ significantly compared to the $M(T)$ of the constituents (e.g. LSMO and SRO). Similar behavior of magnetization is obtained when the magnetic field is applied in the plane (not shown), but the magnetization is larger in the case of the out-of-plane magnetic field. The onset of spontaneous magnetization in all

superlattices occurs at $T=340$ K. The behavior of $M(T)$ at $T<340$ K is significantly different from that of the pure LSMO. For example, the FC magnetization of the sample with $n=2$ decreases gradually as the temperature is raised from 10 K to 33 K. This trend is followed by an increase of magnetization till a maximum value is reached at 100 K. A further increase in temperature leads to a monotonic drops in magnetization (see Fig. 3a). As the SRO layer thickness is increased up to 4 u.c., the magnetization increases slowly above 10 K, becomes maximum at 60 K, and then above 60 K decreases slowly. Between 160 K and 200 K, the magnetization shows a plateau. Two characteristic temperatures can be identified in Fig. 3 in addition to the T_C (350 K) above which the sample becomes paramagnetic. The first one is the temperature (T_C^*) at which the SRO layer becomes ferromagnetic since the magnetization rises sharply below this temperature (150 K). The second one, is the temperature (T_N) below which the magnetization decreases although both the components are in the ferromagnetic state. To clarify this point we have enlarge the $M(T)$ curve in this region and shown them in Fig.3, panel f, g, h, i, and j for superlattice with $n=2, 4, 5, 6$ and 7, respectively.

The distinct cusp in magnetization below the T_C of SRO is an indication of an antiferromagnetic behavior. Thus, we denote the temperature associated to this feature as the Néel temperatures (T_N). However, when the SRO layer thickness is increased beyond 7 u.c., this cusp-like feature below the Curie temperature of SRO is suppressed. The T_C (LSMO), T_C^* and T_N of the superlattices extracted from Fig. 2 are plotted as a function of d_{SRO} in Fig. 4. As discussed before, the T_C of the superlattices is nearly independent of d_{SRO} , and is close to the T_C of LSMO (~ 340 K), while the T_C^* increases with d_{SRO} . However, this T_C^* is not distinguishable for the superlattices with $d_{SRO}>8$ u.c. On the contrary, for the samples with $n<5$ u.c., the T_N shows a distinct increase with the SRO layer thickness. The presence of a distinct $T_C(\text{SRO})$ at 150 K in the $M(T)$ data of the superlattice with $n \geq 4$ indicates the formation of a stoichiometric SRO layer. This observation suggests that in this magnetic system the interface roughness caused by the magnetic and structural disorder is small (~ 2 u.c.). The reproducible ZFC in-plane and out-of-plane minor hysteresis loops of these samples in their corresponding FC state indicate the existence of an antiferromagnetic exchange coupling, but do not show the presence of an interfacial antiferromagnetic layer.⁸ The drop in magnetization, at a temperature which we have marked T_N , could be due to this disordered interface. A similar AFM exchange coupling has been observed in

LSMO/SCRO/LSMO trilayers by Uozu et. al.⁹, and in LSMO/SRO bilayers by Ke and coworkers⁸. While the former group has attributed the AF coupling to superexchange interaction, Ke et. al. attribute it to interfacial charge transfer. However, the AFM exchange coupling with the SRO layer thickness as seen in the present case suggests the possibility of other physical processes. Some well established sources affecting the magnetic coupling in superlattices are the substrate-induced strains, interfacial stress and interlayer exchange coupling.^{13,14} The larger value of T_C^* compare to the transition temperature of SRO could also be due to the high paramagnetic susceptibility¹⁵ of SRO above the $T_C(\text{SRO})$ and/or the reconstruction of the spin state of Ru and Mn ions at/close to the interfaces. The value of the T_N increases and saturates to a temperature $T_C(\text{SRO})$ at higher d_{SRO} , indicating the influence of the size effect of the SRO layer.

In order to study the possible magnetic configuration of Ru and Mn ions at 10 K, we have measured the ZFC magnetic hysteresis loop of these samples with the magnetic field oriented along the [100] and [001] directions of the substrate. The in-plane and out-of-plane ZFC magnetic hysteresis loops of two samples are shown in Fig. 5a. The in-plane and out-of-plane saturation magnetizations (M_S) of all samples are the same though their in-plane and out-of-plane saturation magnetic fields are different. The M_S of some samples, extracted from their ZFC in-plane and out-of-plane hysteresis loop after correcting for the weak diamagnetic response of the substrate, are shown in the Fig. 5b. This figure also includes the theoretical value of M_S calculated from the spin-only M_S of the LSMO ($3.34 \mu_B/\text{Mn}$)¹⁶ and SRO ($1.6 \mu_B/\text{Ru}$)¹⁷. The higher value of the measured M_S , as compared to the theoretical one for the sample with $n = 2$ to 7, indicates an enhancement of the magnetization.

The enhance magnetization could be due to the modification of the charge states of the Ru and Mn ions¹⁸ at the interfaces, and thereby an increase in the effective thickness of the interfacial layer in superlattice with the lower d_{SRO} (< 4 u.c.). In samples with $d_{\text{SRO}} > 4$, the effective thickness of the interfacial layer decreases as the stoichiometric SRO layer start to form. The interfacial magnetic roughness seems to suppressed completely by the strong long range ordering of the ferromagnetic moments of SRO and LSMO at still larger d_{SRO} . However, measurements using electron energy loss spectroscopy should be perform to verify the valency assumptions, in particular the stabilization of the Ru^{5+} spin state.

We have demonstrated that in $\text{La}_{0.7}\text{Sr}_{0.3}\text{MnO}_3$ and SrRuO_3 superlattices an antiferro-

magnetic coupling and increase magnetization can be induced by changing the SRO layer thickness. We attribute these changes to interfacial magnetic and electric disorder, which appears to heal as the SRO layer thickness increases and long range ordering of the magnetic moment associated with Ru ions becomes dominant.

We thank the financial support from the Centre Franco-Indien pour la Promotion de la Recherche Avancee/Indo-French Centre for the Promotion of Advance Research (CE-FIPRA/IFCPAR) under Project No 2808-1. Partial support from the European Union under the STREP research project CoMePhS (N°517039) is also acknowledged.

-
- ¹ J. Nogues and I. K. Schuller, J. Magn. Magn. Mater. 192, 203 (1999).
- ² I. Panagiotopoulos, C. Christides, M. Pissas and D. Niarchos, Phys. Rev. B 60, 485 (1999).
- ³ P. Padhan and W. Prellier, Phys. Rev. B 72, 104416 (2005).
- ⁴ P. Padhan and W. Prellier, Eur. Phys. J. B 45, 169 (2005).
- ⁵ K. Ueda, H. Tabata and T. Kawai, Science 280, 1064 (1998).
- ⁶ K.S. Takahashi, M. Kawasaki and Y. Tokura, Appl. Phys. Lett. 79, 1324 (2001).
- ⁷ P. Padhan, P. Murugavel and W. Prellier, Appl. Phys. Lett. 87, 022506 (2005).
- ⁸ X. Ke and M. S. Rzchowskia, J. Belenky and C. B. Eom, Appl. Phys. Lett. 84, 5458 (2004).
- ⁹ Y. Uozu, T. Nakajima, and M. Nakamura, Y. Ogimoto, M. Izumi and K. Miyano, Appl. Phys. Lett. 85, 2875 (2004).
- ¹⁰ see at: http://ccp14.sims.nrc.ca/ccp/ccp14/ftp-mirror/diffax/pub/treacy/DIFFaX_v1807/
- ¹¹ J.-H. Park, E. Vescovo, H.-J. Kim, C. Kwon, R. Ramesh and T. Venkatesan, Nature 392, 794 (1998).
- ¹² G. Cao, S. McCall, M. Shepard, J. E. Crow and R. P. Guertin, Phys. Rev. B 56, 321 (1997).
- ¹³ K.R. Nikolaev, A. Dobin, I.N. Krivorotov, W.K. Cooly, A. Bhattacharya, A.L. Kobrinskii, L.I. Glazman, R.M. Wentzovitch., E. Dan Dahlberg and A.M. Goldman, Phys. Rev. Lett., 85, 3728 (2000).
- ¹⁴ P. Padhan, R.C. Budhani and R.P.S.M. Lobo, Europhys. Lett. 63, 771 (2003).
- ¹⁵ G. A. Mulhollan, R. L. Fink, J. L. Erskine and G. K. Walters, Phys. Rev. B 43, 13645 (1991).
- ¹⁶ G. Banach, R. Tyer and W. M. Temmerman, J. Magn. Magn. Mater. 272, 1963 (2004).
- ¹⁷ D. Singh, J. Appl. Phys. 79, 4818 (1996).
- ¹⁸ C. Martin, A. Maignan, M. Hervieu, C. Autret, B. Raveau and D. I. Khomskii, Phys. Rev. B, 63, 174402 (2001).

Figure captions:

Figure 1: The experimental (solid line) and simulated (DIFFaX) (dotted line) - 2 x-ray diffraction profiles of the superlattice with $n=4$ and 8. The (001) Bragg's reflection of STO and several orders ($0, \pm 1, \pm 2$) of satellite peaks are indexed.

Figure 2: Temperature dependence of the out-of-plane magnetization under 0.01 tesla field for a 20 u.c. thick film of LSMO (panel a) and SRO (panel b).

Figure 3: Temperature dependence of the out-of-plane magnetization under 0.01 tesla field of the superlattices with $n=2, 4, 5, 6$ and 7 (panels a, b, c, d and e, respectively, for 0-300K and panels f, g, h, i, and j, respectively, for the enlarge part corresponding to the temperature range where the LSMO and SRO are ferromagnetic (panel f, g, h, i, and j respectively). The arrows indicate the T_C and T_N .

Figure 4: Evolution of the T_C , T_C^* and T_N (panel a, b and c respectively) of several superlattices as a function of the SRO layer thickness. In panel a and b the solid lines represent the T_C of bulk LSMO and SRO, respectively, while in panel c the solid line is only a guide to the eyes. Both T_C and T_C^* have been calculated from the intersection of the slope around the transition of magnetization.

Figure 5: (a) ZFC magnetization loop for the (20 u.c.)LSMO/(n u.c.)SRO superlattice with $n = 4$ and 12. Magnetic field is oriented along the $[100]$ and $[001]$ directions of STO. (b) : Experimental and theoretical saturation magnetization for the superlattices as a function of the SrRuO_3 layer thickness. The solid lines are guide to the eyes.

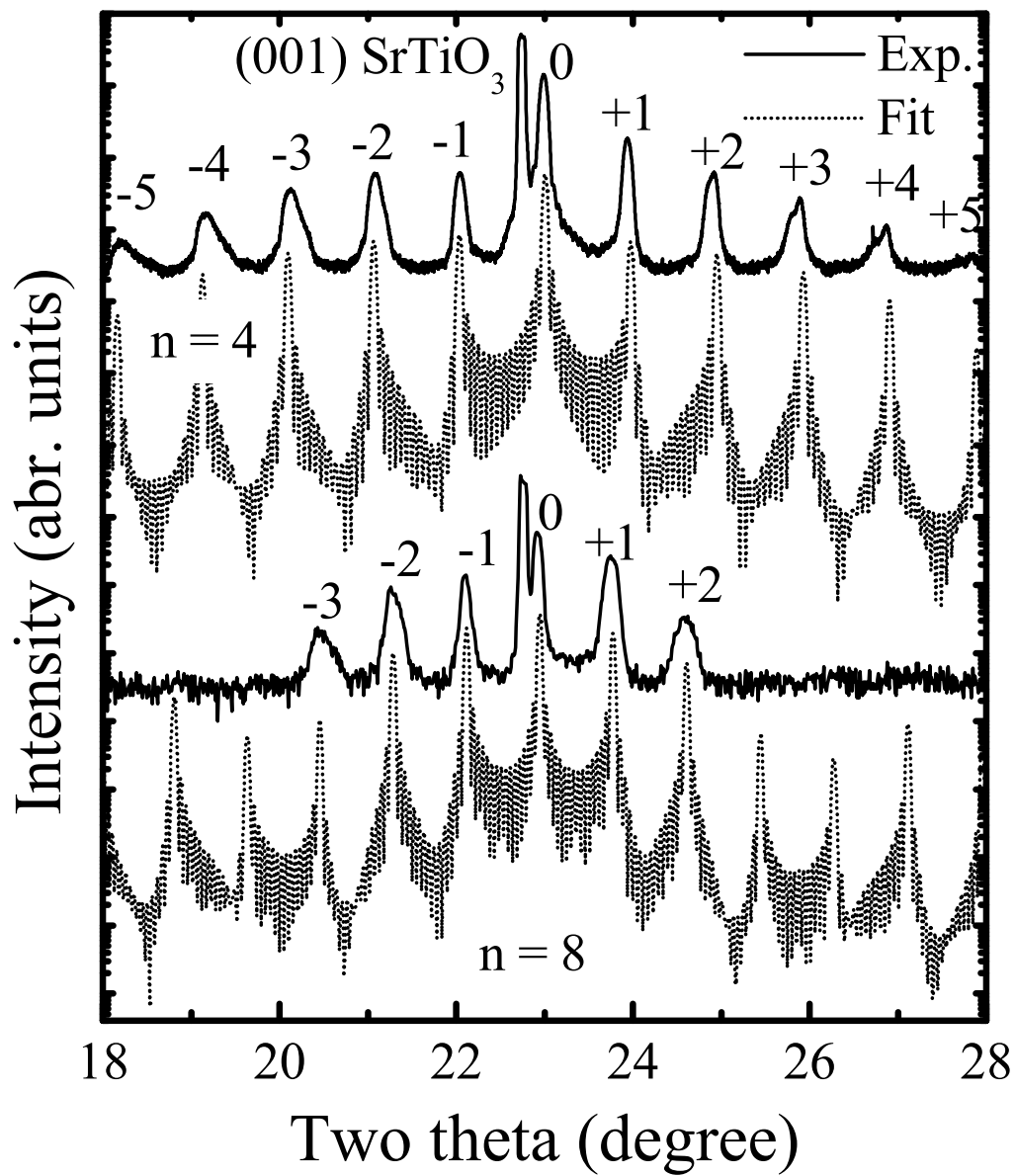


FIG. 1: Padhan et. al.

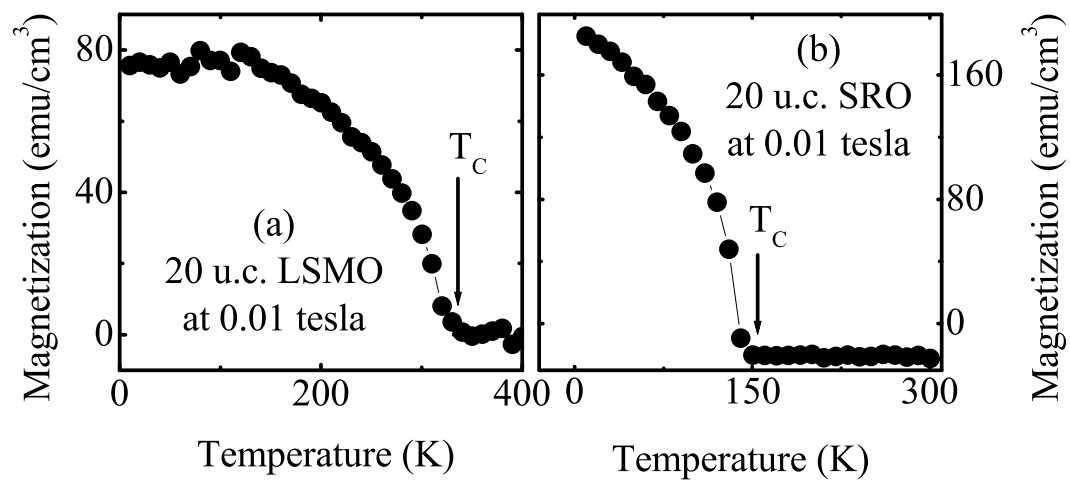


FIG. 2: Padhan et. al.

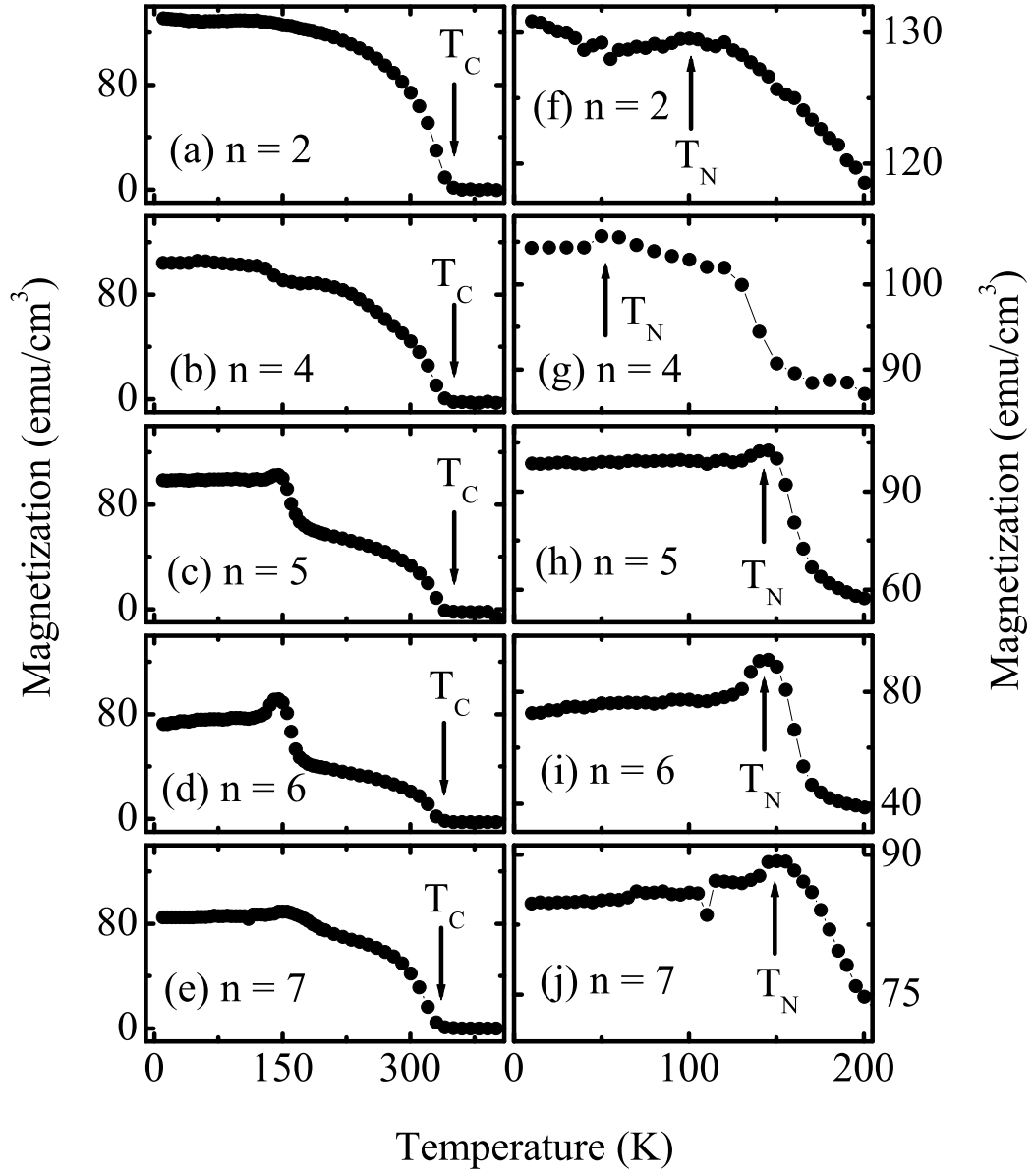


FIG. 3: Padhan et. al.

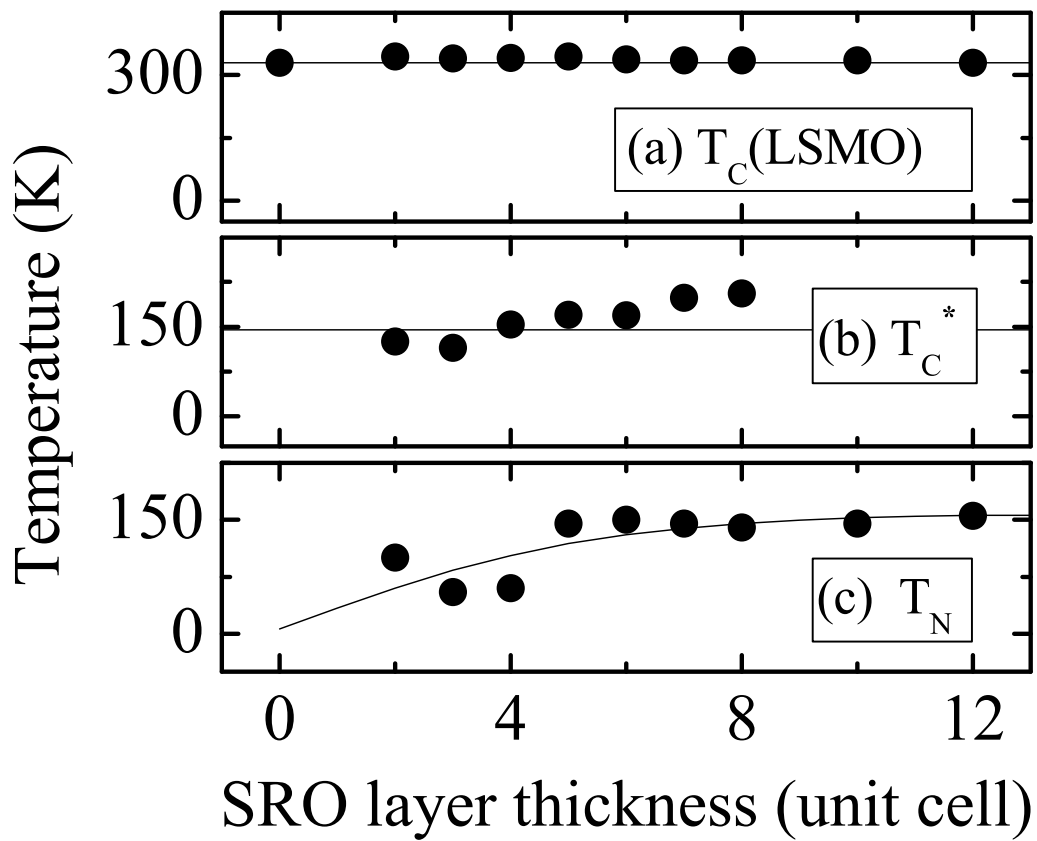


FIG. 4: Padhan et. al.

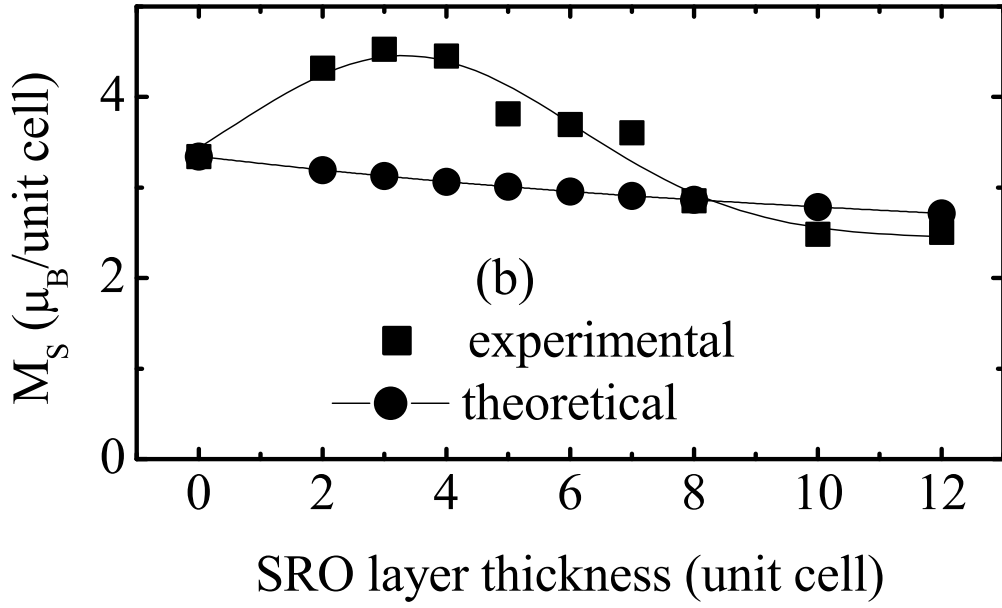
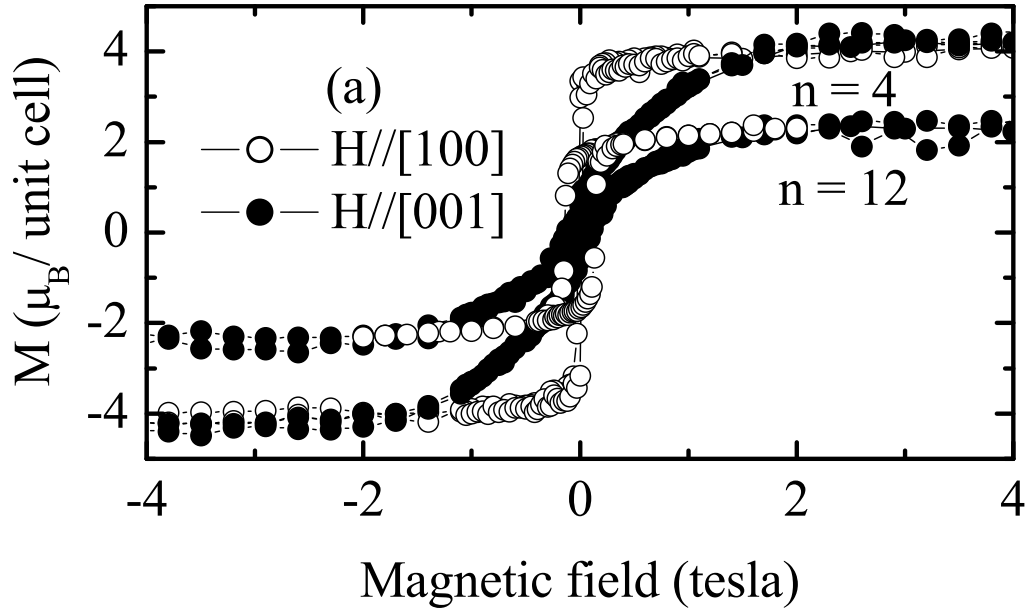


FIG. 5: Padhan et. al.